

# The surface barrier in mesoscopic type I and type II superconductors

Alexander D. Hernández<sup>1,2</sup> and Daniel Domínguez<sup>2</sup>

<sup>1</sup>Laboratorio de Superconductividad, Facultad de Física-IMRE, Universidad de la Habana, 10400, Ciudad Habana, Cuba.

<sup>2</sup>Centro Atómico Bariloche, 8400 San Carlos de Bariloche, Río Negro, Argentina

We study the surface barrier for magnetic field penetration in mesoscopic samples of both type I and type II superconductors. Our results are obtained from numerical simulations of the time-dependent Ginzburg-Landau equations. We calculate the dependence of the first field for flux penetration ( $H_p$ ) with the Ginzburg-Landau parameter ( $\kappa$ ) observing an increase of  $H_p$  with decreasing  $\kappa$  for a superconductor-insulator boundary condition  $((\nabla - iA)\Psi|_n = 0)$  while for a superconductor-normal boundary condition (approximated by the limiting case of  $\Psi|_S = 0$ )  $H_p$  has a smaller value independent of  $\kappa$  and proportional to  $H_c$ . We study the magnetization curves and penetration fields at different sample sizes and for square and thin film geometries. For small mesoscopic samples we study the peaks and discontinuous jumps found in the magnetization as a function of magnetic field. To interpret these jumps we consider that vortices located inside the sample induce a reinforcement of the surface barrier at fields greater than the first penetration field  $H_{p1}$ . This leads to multiple penetration fields  $H_{pi} = H_{p1}, H_{p2}, H_{p3}, \dots$  for vortex entrance in mesoscopic samples. We study the dependence with sample size of the penetration fields  $H_{pi}$ . We explain these multiple penetration fields extending the usual Bean-Livingston analysis by considering the effect of vortices inside the superconductor and the finite size of the sample.

PACS numbers: 74.20.De, 74.25.Ha, 74.60.Ec

## I. INTRODUCTION

In the last years there has been an important experimental and theoretical interest in the study of vortex physics in a mesoscopic scale.<sup>1-4</sup> The smallness of these systems imply that the sample geometry and the interaction between the vortices and the sample surface become important. The interaction between vortices and the surface manifests itself fundamentally in the existence of a surface barrier, first studied by Bean and Livingston,<sup>5</sup> which delays the vortex penetration and generates metastable states. If the surface effects are ignored, the penetration of magnetic field is energetically favorable at the first critical field  $H_{c1}$ . However the energy barrier of the surface prevents the vortex entry until a higher field  $H_p$  at which the barrier vanishes.  $H_p$ , also known as the superheating field, is associated with the peak in the magnetization curves and is strongly influenced by the presence of surface irregularities.

The surface barrier has attracted a renewed interest recently in the study of mesoscopic superconductors. For example, Enomoto and Okada<sup>6</sup> by means of numerical simulations of the time-dependent Ginzburg-Landau equations (TDGL), studied the influence of temperature and surface irregularities on the surface barrier. Sonin and Traito<sup>7</sup> showed that the presence of the surface barrier affects the entry and exit of vortices influencing the surface resistance. They found a surface-induced suppression of the ac losses.

One important line of research of mesoscopic superconductors are the superconducting disks.<sup>1,2,4,8-14</sup> The study of small superconducting disks was started by Buisson *et al.*<sup>1</sup> for disks with radius  $\sim 7 \mu\text{m}$ . Recent advances in the microfabrication technology and measure-

ment techniques now allow the fabrication and study of superconducting disks with sizes comparable to the coherence length  $\xi$ , with radius as small as  $0.3 \mu\text{m}$ .<sup>2</sup> Most of the studies were done in Al disks, a material with  $\kappa \simeq 0.3$ , however for small samples the effective penetration depth  $\Lambda = \lambda^2/d$  increases for decreasing disk thickness ( $d$ ) resulting in effective  $\kappa$  values in the type II region that can be studied theoretically using the equilibrium Ginzburg-Landau equations. In this regime the Al disk can develop Abrikosov multivortex states<sup>9</sup> and depending on the radius ( $R$ ) and thickness of the disk it is possible to observe first or second order phase transitions,<sup>8</sup> by increasing the disk sizes the second order reversible phase transition observed for small disk radius is replaced by a first order transition. There is also an intermediate regime where jumps in the magnetization appear associated with the vortex entrance. Other interesting phenomena have been studied for mesoscopic Al disks, for example in Ref. 14 hysteresis in the magnetization curves was observed experimentally and explained in terms of the presence of a “Bean-Livingston” surface barrier and in Ref. 12 the behavior of the third critical field  $H_{c3}$  was investigated for different sample sizes and geometries.

The time dependent Ginzburg-Landau (TDGL) equations have been proposed<sup>15</sup> as a time dependent generalization of the mean field approach of the Ginzburg-Landau theory. Gorkov and Eliashberg<sup>16</sup> obtained the TDGL equations from the microscopic BCS theory in the gapless case. In the last years, numerical simulations of the time dependent Ginzburg-Landau (TDGL) equations have been successfully used to study the magnetic properties and flux dynamics in superconductors.<sup>17-22</sup> Frahm *et al.*<sup>17</sup> and Liu *et al.*<sup>18</sup> simulated the TDGL equations for  $\kappa = 0.3 - 20$ , Kato *et al.*<sup>19</sup> and Machida and Kaburaki<sup>20</sup>

for  $\kappa = 2$ , Aranson *et al.*<sup>21</sup> studied vortex dynamics in the  $\kappa = \infty$  limit, and Vicente-Álvarez *et al.* studied the dynamics of  $d$ -wave superconductors.<sup>22</sup> Only few studies of the TDGL equations have been done in superconductors with type I behavior,<sup>17,18</sup> possibly because the theory is better to describe a superconductor near a second order phase transition at a temperature near  $T_c$ .

In this paper, we present a numerical simulation of the TDGL equations to study the surface barrier in mesoscopic samples for  $\kappa = 0.15 - 2$ . We neglect demagnetization effects and therefore we assume that the sample is infinite in the direction of the external magnetic field (the  $\hat{z}$  direction). We consider square samples that are mesoscopic in the  $xy$  plane (perpendicular to the magnetic field) with linear sizes of  $5 - 30\lambda$ , with  $\lambda$  the penetration depth.

The paper is organized as follows. In Sec.II we present the TDGL equations with their discretized form in finite differences, and we discuss their possible boundary conditions. In the Sec.III of the paper we study the dependence of the penetration field  $H_p$  with the Ginzburg-Landau parameter  $\kappa$  ( $\kappa = \lambda/\xi$ ), exploring both the type I ( $\kappa < 1/\sqrt{2}$ ) and the type II region ( $\kappa > 1/\sqrt{2}$ ) for large samples. We study the effects of the surface barrier from a comparison of two types of boundary conditions. (i) The superconductor-insulator (S-I) boundary condition: consisting in the vanishing of the superconducting current perpendicular to the boundary ( $\mathbf{J}_s \cdot \hat{\mathbf{n}} = 0$ ). In this case we find an increase of  $H_p$  with decreasing  $\kappa$ . (ii) The superconductor-normal (S-N) boundary condition: approximated as the vanishing of the superconducting order parameter at the boundary ( $\Psi|_S = 0$ ). A different behavior is observed for the S-N boundary condition, the field  $H_p$  is independent of  $\kappa$  and nearly equal to  $H_c$ . In the Sec.IV we study the surface barrier in mesoscopic superconductors. In particular, in Sec.IVA we study magnetization curves in type II superconductors at different sample dimensions in the region where the transition from a macroscopic to a mesoscopic behavior takes place. In Sec.IVB we show that the discontinuities that appear in the magnetization curves of mesoscopic samples can be explained by considering that the vortices that are inside the sample induce a reinforcement of the surface barrier at fields greater than the first penetration field. In this way, it is possible to define a second, third, fourth, etc. penetration fields which are a consequence of the interaction between vortices and the surface currents. We study the sample size dependence of the first, second and third penetration fields and we show that for sufficiently large sample sizes the known macroscopic behavior is recovered, i.e. a continuous magnetization curve appears since  $H_{p3} \rightarrow H_{p2} \rightarrow H_p$ . Finally in Sec.V we give a summary of our results and conclusions.

## II. MODEL AND DYNAMICS

### A. TDGL equations

Our numerical simulations are carried out using the time-dependent Ginzburg-Landau equations complemented with the appropriate Maxwell equations. In the zero-electric potential gauge we have:<sup>15,23</sup>

$$\frac{\partial \Psi}{\partial t} = \frac{1}{\eta} [(\nabla - iA)^2 \Psi + (1 - T)(1 - |\Psi|^2)\Psi] \quad (1)$$

$$\frac{\partial A}{\partial t} = (1 - T)\text{Im}[\Psi^*(\nabla - iA)\Psi] - \kappa^2 \nabla \times \nabla \times A \quad (2)$$

where  $\Psi$  and  $A$  are the order parameter and vector potential respectively and  $T$  is the temperature.<sup>24</sup> Equations (1) and (2) are in their dimensionless form. Lengths have been scaled in units of  $\xi(0)$ , times in units of  $t_0 = 4\pi\sigma\lambda^2/c^2 = \xi(0)^2/\eta D$ ,  $A$  in units of  $H_{c2}(0)\xi(0)$  and temperatures in units of  $T_c$ .  $\eta$  is proportional to the ratio of characteristic times for  $\Psi$  and  $A$ ,  $\eta = t_\Psi/t_0 = c^2/(4\pi\sigma\kappa^2 D)$ , with  $t_\Psi = \xi^2/D$ , where  $\sigma$  is the quasiparticle conductivity and  $D$  is the electron diffusion constant. For superconductors with magnetic impurities we have  $D = c^2/(48\pi\kappa^2\sigma)$ , and therefore  $\eta = 12$  in this case.

We have used the standard finite difference discretization scheme to solve equations (1) and (2).<sup>23</sup> The order parameter and vector potentials are defined at the nodes of a rectangular mesh ( $\vec{r} = (I, J)$ ), and the link variables  $U_{\mu I, J} = \exp(-i\kappa h_\mu A_{\mu I, J})$  ( $\mu = x, y$ ) are introduced in order to maintain the gauge invariance under discretization.

In our simulations we have assumed a sample that has a square/rectangular shape in the  $x, y$  direction with dimensions  $L_x \times L_y$  and it is infinite in the  $z$  direction. We apply the magnetic field parallel to the  $z$  direction, the symmetry of the problem then implies for all mesh points  $A_{I, J} = (A_{xI, J}, A_{yI, J}, 0)$  and  $\mathbf{B}_{I, J} = (0, 0, B_{zI, J})$ , where  $B_{zI, J} = (\nabla \times \vec{A})_z = (\partial_x A_{yI, J} - \partial_y A_{xI, J})$ .

In this geometry the discretized form of equations (1) and (2) are:

$$\begin{aligned} \frac{\partial \Psi}{\partial t} = & \frac{1}{\eta} \left( \frac{U_{xI, J} \Psi_{I+1, J} - 2\Psi_{I, J} + U_{xI-1, J} \Psi_{I-1, J}}{(\Delta x)^2} + \right. \\ & + \frac{U_{yI, J} \Psi_{I, J+1} - 2\Psi_{I, J} + U_{yI, J-1} \Psi_{I, J-1}}{(\Delta y)^2} + \\ & \left. + (1 - \frac{T}{T_c})(1 - |\Psi_{I, J}|^2)\Psi_{I, J} \right) \end{aligned} \quad (3)$$

$$\begin{aligned} \frac{\partial A_{xI, J}}{\partial t} = & (1 - \frac{T}{T_c}) \frac{\text{Im}[U_{xI, J} \Psi_{I, J}^* \Psi_{I+1, J}]}{\Delta x} - \\ & - \kappa^2 \left( \frac{B_{zI, J} - B_{zI, J-1}}{\Delta y} \right) \end{aligned} \quad (4)$$

$$\begin{aligned} \frac{\partial A_{yI, J}}{\partial t} = & (1 - \frac{T}{T_c}) \frac{\text{Im}[U_{yI, J} \Psi_{I, J}^* \Psi_{I, J+1}]}{\Delta y} - \\ & - \kappa^2 \left( -\frac{B_{zI, J} - B_{zI-1, J}}{\Delta x} \right) \end{aligned} \quad (5)$$

where  $\Delta x$  and  $\Delta y$  are the mesh widths of the spatial discretization.

## B. Boundary conditions

The dynamical equations must be complemented with the appropriate boundary conditions for both the order parameter and the vector potential.

The boundary conditions for the vector potentials  $A_{\mu I, J}$  are obtained by making

$$B = \nabla \times A = H_a$$

at the sample surface (where  $H_a$  is the applied magnetic field).

The boundary conditions for the order parameter depend sensibly on the physical nature of the boundary. In general is given by:<sup>25</sup>

$$(\vec{\Pi}\Psi)|_n = (\nabla - i\vec{A})|_n \Psi = \frac{\Psi}{b} \quad (6)$$

where  $b$  is a surface extrapolation length which embodies the surface suppression (or enhancement if  $b < 0$ ) of the superconducting order parameter.

For the boundary between a superconductor and an insulator (or the vacuum) we have  $b \sim \xi^2(0)/a$ , with  $a$  the interatomic distance.<sup>25</sup> For low temperature superconductors  $b$  is huge ( $\sim 1\text{cm}$ ), and the superconductor-insulator (S-I) boundary condition is usually approximated with the limit  $b \rightarrow \infty$ :

$$(\nabla - i\vec{A})|_n \Psi = 0 \quad (7)$$

This boundary condition implies that the perpendicular component of the superconducting current is equal to zero at the surface ( $\vec{J}_s|_n = 0$ ). This is the most frequently used boundary condition because it also minimizes the free energy at the sample surface. More precisely, this boundary condition is valid for superconductors with interfaces for which  $b \gg \xi(T)$ .

For the boundary between a superconductor and a normal metal we have  $b \sim \frac{N}{N_N} \frac{1}{T_j} \frac{\xi(0)^2}{\xi_N}$ , with  $N$  the local density of states at the Fermi surface,  $N_N$  the bulk density of states,  $T_j$  the transmission coefficient at the boundary and  $\xi_N$  is the coherence length in the normal state.<sup>25</sup> Typically  $(N_N/N)T_j \sim 1$  and  $b$  is small when compared to  $\xi(T)$ . Therefore, the superconducting-normal (S-N) boundary condition can be approximated by  $b \approx 0$ , giving:

$$\Psi|_S = 0. \quad (8)$$

The case of  $b \rightarrow 0$  is also found for a ferromagnet-superconductor surface.<sup>26</sup> Moreover, the condition  $\Psi|_S = 0$  is similar to having a high density of defects at the interface and therefore a highly defective surface is also represented by (8). It is also interesting to note that for high  $T_c$  superconductors even the superconductor-insulator boundary is better approximated by (8) since  $b \sim \xi(0)^2/a \ll \xi(T)$  in a large range of temperatures,

due to the smallness of  $\xi(0)$  in this case. The boundary condition of (8) completely suppresses the currents at the boundary ( $\vec{J}_s^\perp = \vec{J}_s^\parallel = 0$ ) and maximizes the surface Helmholtz free energy, which becomes equal to the free energy of a normal metal.

In the study of the surface barrier in Sec.III we will compare these two conceptually different boundary conditions of the order parameter. They represent the two limiting cases of Eq. (6) and we will call them, in short, the “S-I” boundary condition (Eq. (7)) and the “S-N” boundary condition (Eq. (8)). A previous discussion of these two types of boundary conditions was done by Buisson *et al.*<sup>1</sup>, where the equilibrium solutions and eigenvalues of the linearized Ginzburg-Landau equations were compared to study the behavior near  $H_{c2}$ . However, for the vortex nucleation process at low magnetic fields the nonlinear terms of the Ginzburg-Landau equations should be considered.

## III. SURFACE BARRIER IN MACROSCOPIC SAMPLES

When the magnetic field  $H$  is increased starting from  $H = 0$  in a finite sample, the Meissner state is destroyed at a magnetic field  $H_p$  which is typically higher than  $H_{c1}$ . This is due to the presence of a surface barrier for vortex entrance in finite samples. The surface barrier in macroscopic samples is sometimes known as the “Bean-Livingston barrier” since it was first studied by Bean and Livingston (BL)<sup>5</sup>. In the BL work the surface barrier was obtained in the London approximation and for the ideal case of a semi-infinite superconductor, therefore vortex core nucleation effects and geometrical effects were both neglected. With this simplification, the BL work was able to identify one of the most relevant causes of the surface barrier: the screening currents near the surface circulate in the opposite direction to the superconducting currents around a vortex. This is typically viewed as a competition between the repulsion between the vortex and the surface shielding current and the attractive force between a vortex inside the sample and its image. This argument, which is based on the London model, yields the Bean-Livingston result for the penetration field,  $H_p^{\text{London}} \approx \frac{\sqrt{2}}{2} H_c$ , which is independent of  $\kappa$ .<sup>5,25</sup> However, in addition to overcoming the barrier induced by the shielding Meissner currents, a vortex penetration event has also to deplete the superconducting order parameter  $|\Psi|$  at the surface, resulting in a higher penetration field  $H_p(\kappa) > H_p^{\text{London}}$ .<sup>30–35</sup> This later effect can be sensitive to the boundary conditions of the Ginzburg-Landau equations. In this section we will discuss the effect of boundary conditions on the surface barrier in macroscopic samples as a function of  $\kappa$ .

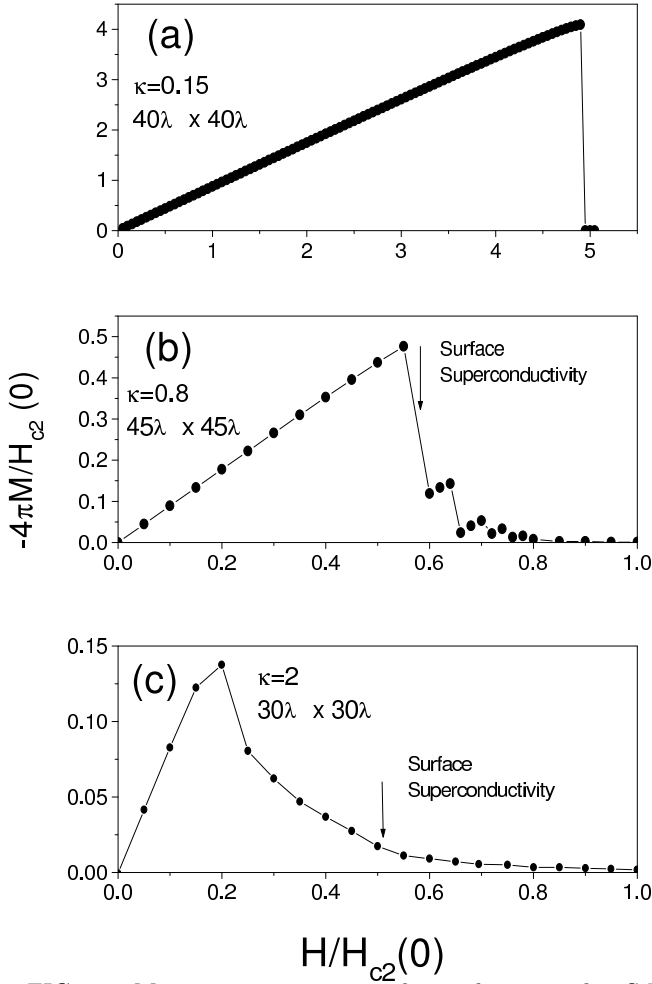


FIG. 1. Magnetization curves obtained using the S-I boundary condition: (a)  $\kappa = 0.15$ , (b)  $\kappa = 0.8$  and (c)  $\kappa = 2$ . (Inserted in the figure are the size of the superconducting region used in the simulation,  $\lambda$  is the penetration length).

We start our study of the surface barrier by first analyzing the magnetization curves in large samples. The magnetization curves for the S-I boundary condition are summarized in Fig.1 and for the S-N boundary condition are summarized in Fig.2. In both cases the curves were obtained initializing the variables to a perfect Meissner state [ $\Psi(I, J, t = 0) = 1$  and  $A(I, J, t = 0) = 0$ ] and increasing the magnetic field at subsequent steps, usually with  $\Delta H = 0.05 H_{c2}$ . We take as the initial condition at a magnetic field  $H$  the final state of  $\Psi(I, J)$  and  $A(I, J)$  of the previous magnetic field value  $H - \Delta H$ . In this way we mimic the experimental procedure of increasing the magnetic field in a magnetization measurement. For each magnetic field we calculate the magnetization  $M$  taking time averages of the time dependent magnetization  $M(t)$ :

$$4\pi M(t) = \frac{\Delta x \Delta y}{L_x L_y} \sum_{I,J} B_z(I, J, t) - H_a$$

$$M = \frac{\Delta t}{t_f - t_0} \sum_{t=t_0}^{t_f} M(t), \quad (9)$$

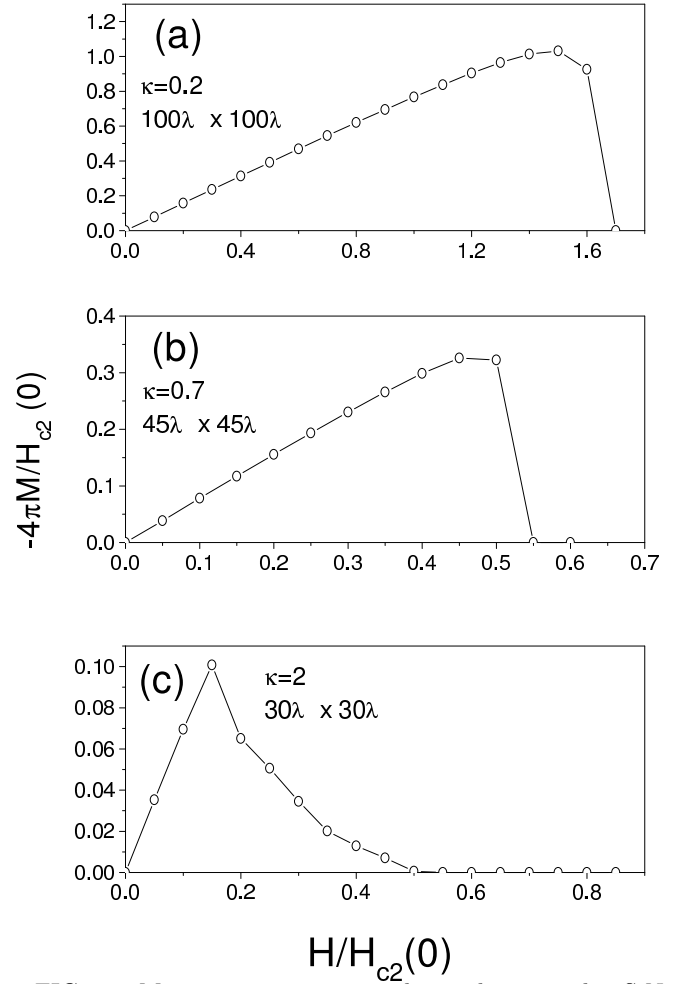


FIG. 2. Magnetization curves obtained using the S-N boundary condition: (a)  $\kappa = 0.2$ , (b)  $\kappa = 0.7$  and (c)  $\kappa = 2$ .

where we start the average at a time  $t_0$  after a steady state was reached. In the simulations we have taken  $T = 0.5$ ,  $\eta = 12$  and we used a mesh of  $120 \times 120$  points. In order to make efficient calculations we have chosen the time step ( $\Delta t$ ) and the spatial discretization ( $\Delta x$  and  $\Delta y$ ) depending on the value of  $\kappa$ . For example, for  $\kappa = 0.15$  we used  $\Delta x = \Delta y = 0.05$  and  $\Delta t = 0.0025$ ; for  $\kappa = 0.8$ ,  $\Delta x = \Delta y = 0.3$  and  $\Delta t = 0.0025$  and for  $\kappa = 2$ ,  $\Delta x = \Delta y = 0.5$  and  $\Delta t = 0.015$ . Since the TDGL equations considered here represent a mean field dynamics,<sup>15–18,20,21,23</sup> the effect of thermal noise fluctuations beyond mean field are neglected,<sup>24</sup> which is correct for low  $T_c$  superconductors.

Figure 1(a) shows the case of a type I superconductor with  $\kappa = 0.15$ . We can see that the TDGL equations reproduce the basic phenomenology of type I superconductivity characterized by a first-order magnetic transition. In this case the superconductivity disappears abruptly and there is no surface superconductivity. The field profile is described by a Meissner state and  $H = H_a \exp(-x/\lambda)$ . In this simulation the intermediate state structures typical of type I superconductors are not found at equilibrium<sup>27</sup> since the long range in-

interactions between currents and demagnetization effects are neglected.<sup>28,29</sup> Results for a type II superconductor with  $\kappa = 2$  are shown in Figure 1(c). In this case the superconductor is in the Meissner state until a penetration field  $H_p$  is reached. At  $H_p$  some vortices enter the sample and a peak in the magnetization curve is observed. Above  $H_p$  the magnetization increases due to the penetration of vortices in the sample, until the establishment of surface superconductivity for fields in the range  $H_{c3}(T) > H > H_{c2}(T)$ . The criterion for surface superconductivity that we use is the existence of superconductivity in the surface (i.e.  $|\Psi| \neq 0$  in a contour around the surface of width equal to the discretization length,  $\Delta x = 0.5\xi$  in this case) and the exact vanishing of superconductivity in the bulk (i.e.  $|\Psi| = 0$  inside the region enclosed by the surface contour).

The S-N boundary condition leads to a different magnetic behavior as can be observed in Figure 2 where we have used similar parameters as those reported in Figure 1. We observe the following differences: (i) The magnetization is smaller for the same external magnetic field (there are less vortices). Since in this case the superconducting order parameter vanishes at the surface, the Meissner shielding currents are nucleated at a distance of a few  $\xi$  inside the sample, instead of being right at the boundary. Therefore less vortices can stay inside the sample for a given magnetic field when compared with the S-I boundary. For example, for  $\kappa = 2$ , we find that the shielding distance  $\delta$  between the vortices and the sample surface is  $\delta_{SN} \approx 5\lambda$  for the S-N interface while for the S-I interface we have  $\delta_{SI} \approx 3\lambda$ . In the general case, when the boundary condition is described by Eq.(6) with a finite  $b$ , one can expect that the shielding distance will have an intermediate value  $\delta_{SN} > \delta(b) > \delta_{SI}$ . (ii) There is no surface superconductivity above  $H_{c2}$ . This is an obvious and direct consequence of the S-N boundary condition that enforces  $\Psi|_S = 0$ . (iii) The first penetration field  $H_p$  is smaller and therefore the surface barrier is lower, we will discuss this in detail in the following paragraphs.

In order to understand the difference in the surface barrier, let us study the dynamics of the first vortex penetration just at  $H = H_p$ . Figure 3 shows the dynamic evolution of the order parameter near a small region close to an S-I interface (Figure 3 left) and close to an S-N interface (Figure 3 right). If the interface is of the S-I type the order parameter at the boundary is different from zero in the Meissner state. When the condition for vortex entrance is fulfilled the order parameter at a boundary point has to decrease until reaching zero. Therefore there is an intermediate time interval when  $\Psi = 0$  in a point at the boundary. Just in this moment a vortex can enter the sample and afterwards the order parameter at the boundary increases again and returns to a non-zero value. It is interesting to note that this process is always necessary for vortex penetration in S-I interfaces, there is always the need of an intermediate  $\Psi = 0$  state at the boundary. On the contrary, a smooth entrance of vortices is observed for an S-N interface (Figure 3 right).

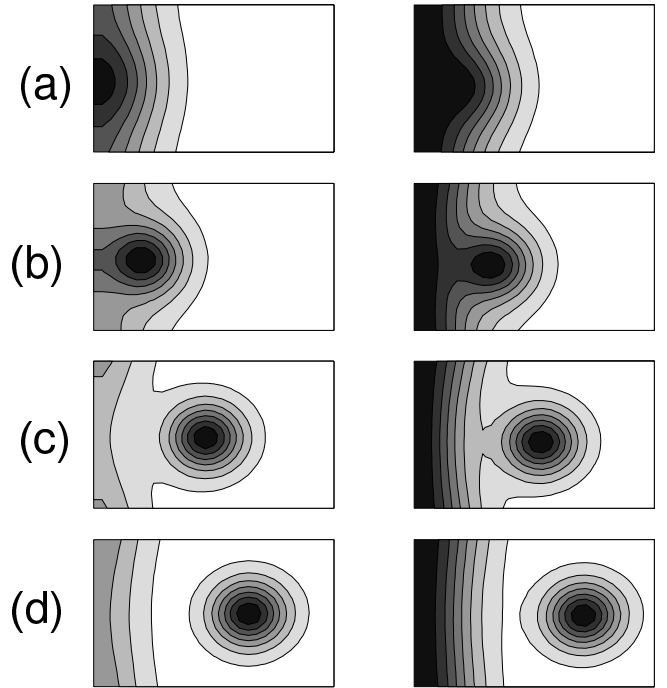


FIG. 3. Time evolution of the spatial pattern of the order parameter in a small region around the boundary where a vortex entrance is taking place. For the S-I condition (left) the magnetic field is  $H = 0.199H_{c2}(0)$ , and for the S-N condition (right)  $H = 0.169H_{c2}(0)$ . In both cases  $H$  is just above the first penetration field and  $\kappa = 2$ . Gray scale from black ( $|\Psi| = 0$ ) to white ( $|\Psi| = 1$ ).

For this boundary condition the order parameter at the interface is already zero. A small deformation of the region of  $\Psi = 0$  allows for the penetration of a vortex. Since there is no need of depressing the order parameter at the boundary, the surface barrier is much smaller in the S-N case. A similar dynamical behavior for vortex entrance would appear in an S-I interface with defects at the surface. At the defects the order parameter is depressed and therefore  $\Psi = 0$  is already established at some boundary points, which are preferred points for vortex entrance.

From the magnetization curves we can obtain the first field for flux penetration  $H_p$  as a function of  $\kappa$  for the different boundary conditions, this is shown in Figure 4. The  $\kappa$  dependence of the superheating field  $H_p$  has been previously calculated for the case of a semi-infinite medium with the Ginzburg-Landau equations.<sup>30–35</sup> Matricon and Saint James<sup>31</sup> obtained  $H_p(\kappa)$  solving the semi-infinite one-dimensional GL equations, in Ref. 32–35 the stability of the superheated state under small fluctuations of the order parameter and the vector potential was discussed, and very recently Vodolazov<sup>36</sup> analyzed the effects of surface defects on  $H_p$ . In the case of a one dimensional semi-infinite medium, the Matricon-Saint James<sup>31</sup> solution can be obtained solving the equations:

$$\frac{d^2\Psi}{\kappa^2 dx^2} = A^2\Psi + \Psi - \Psi^3,$$

$$\frac{d^2 A}{dx^2} = \Psi^2 A \quad (10)$$

with the boundary conditions:

$$\begin{aligned} H &= H_a \text{ and } \frac{d\Psi}{dx} = 0 \text{ at } x = 0 \\ A &= H = 0 \text{ and } \Psi = 1 \text{ at } x = \infty \end{aligned} \quad (11)$$

Solving numerically equations (9) with the boundary condition (10) it is possible to find a relationship among  $H_a$  and  $\Psi(x=0) = \Psi_o$ , where  $H_p$  is the maximum value of  $H_a$  that allows a physically meaningful  $\Psi_o$ , i.e.  $0 < \Psi_o < 1$ . The results obtained in this way are represented by the continuous-line of Figure 4. Our simulation results, on the other hand, are a numerical solution of the exact problem in a two dimensional square sample (which has geometrical effects) and are represented by closed circles. The  $H_p$  values reported here are the peaks of the simulated dc-magnetization curves and the error bars correspond to the discrete field step used in the magnetization curves. We see in Fig. 4 that the value of  $H_p$  obtained for the S-I interface is always well above  $H_{c1}$  in the type II region ( $H_{c1}(T) = [(\ln \kappa)/\sqrt{2}\kappa]H_c(T)$ ) and above  $H_c$  in the type I region, supporting the existence of a “surface barrier” even in the type I case. Our numerical simulations show that for the S-I interface  $H_p$  increases with decreasing  $\kappa$  and  $H_p(\kappa) > H_c$ , with a behavior in good agreement with the result for the semi-infinite medium obtained by Matricon-Saint James. (However, for smaller mesoscopic samples the value of  $H_p$  can be significantly larger than the Matricon-Saint James result, enhancing the geometrical effect of the square sample, see Sec. IV). For  $\kappa \rightarrow 0$  our results agree with the known behavior of the superheating field in type I superconductors,  $H_p \sim 1/\sqrt{\kappa}$ .<sup>30–32</sup> For  $\kappa \rightarrow \infty$  we obtain that  $H_p \rightarrow H_c$  in agreement with the result of Ref. 30–32. Figure 4 also shows that in the type II region the  $H_{c2}$  values obtained from the S-I simulations (closed squares) are close to the expected values ( $H_{c2}(T) = \sqrt{2}\kappa H_c(T)$ , dotted line). Some differences in  $H_{c2}$  appear at small  $\kappa$  near the type I region, since in this region the field  $H_p$  is close to  $H_{c2}$  and a delay of the superconducting-normal transition could be expected.

The behavior of  $H_p$  vs  $\kappa$  is very different when the S-N boundary condition is used. In this case,  $H_p$  is independent of  $\kappa$  and nearly equal to  $H_p^{\text{London}} \propto H_c$  (see the open circles of Figure 4). This result shows that in the case of the S-N interface, when the condition  $\Psi|_S = 0$  is enforced, the surface barrier is only due to the surface shielding currents and well described by the London approximation value of Bean and Livingston:  $H_p^{\text{London}}$ .<sup>5,25</sup> On the other hand, in the case of the S-I interface the penetration field  $H_p$  is higher due to the extra contribution needed for the vanishing of the order parameter at the surface in a vortex penetration event. In a type I superconductor, the “surface barrier” can be interpreted as the barrier for penetration of the normal state from

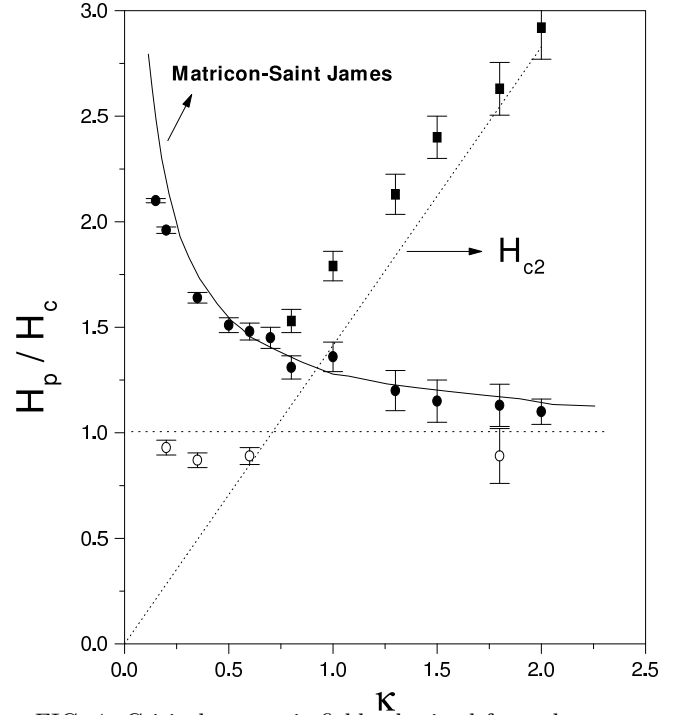


FIG. 4. Critical magnetic fields obtained from the magnetization curves at different  $\kappa$  values. For the S-I boundary condition are plotted the superheating field ( $H_p$ ) (closed circles) and the second critical field ( $H_{c2}$ ) (closed squares). For the S-N boundary condition is plotted  $H_p$  (open circles). The dashed and dotted curves are the expected values of  $H_c$  and  $H_{c2}$  respectively. The continuous line is the result of  $H_p$  vs  $\kappa$  obtained by Matricon and Saint-James for a semi-infinite sample.

the boundary. In the S-N interface of a type I superconductor there is no barrier, i.e.  $H_p = H_c$ , which is an obvious result since the boundary condition already enforces the normal phase ( $\Psi = 0$ ) at the surface. On the contrary, in the S-I interface of a type I superconductor the barrier for nucleation of the normal phase at the boundary can be very high,  $H_p \gg H_c$ , as can be seen in Fig.4.

In the general case, when the boundary condition of a superconducting sample is described by Eq.(6) with a finite  $b$ , we expect that  $H_p(b, \kappa)$  will be in between the two limit cases studied here,  $H_p^{SN}(b=0, \kappa) < H_p(b, \kappa) < H_p^{SI}(b=\infty, \kappa)$ . Ideally, most of the superconductors should be closer to the behavior of  $H_p^{SI}(b=\infty, \kappa)$  but the effect of a finite  $b$  and the presence of defects at the surface will give a smaller value of  $H_p$  with a lower bound given by  $H_p^{SN}(b=0, \kappa)$ .

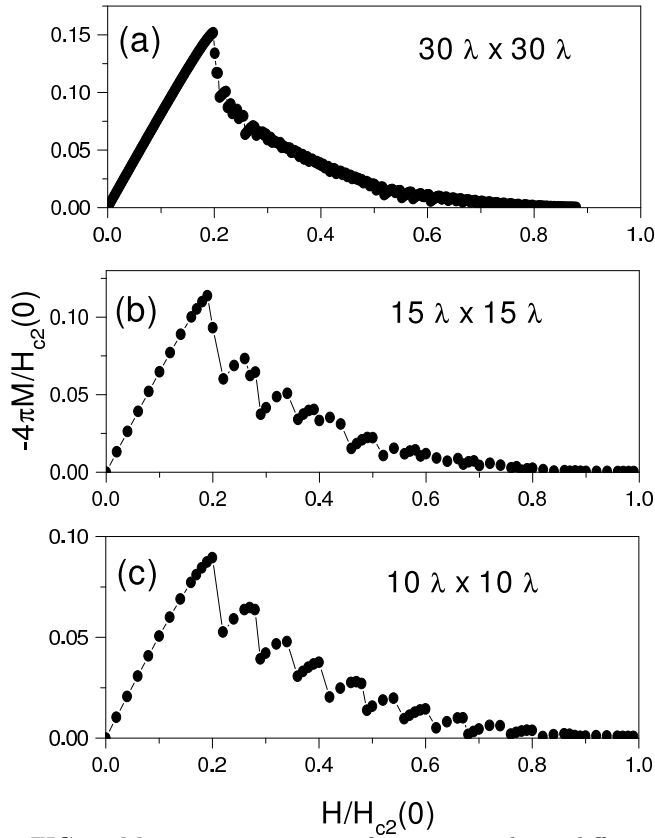


FIG. 5. Magnetization curves of square samples at different sizes and using the S-I boundary condition for  $\kappa = 2$  (a)  $30\lambda \times 30\lambda$ , (b)  $15\lambda \times 15\lambda$  and (c)  $10\lambda \times 10\lambda$ .

#### IV. SURFACE BARRIER IN MESOSCOPIC SAMPLES

##### A. Finite-size effects in mesoscopic type II superconductors

The magnetic behavior of mesoscopic superconductors is different from the behavior of bulk samples. In the mesoscopic scale, several maxima appear in the magnetization curves which are related to the vortex entrance. This result is quite general and appears either in thin films at parallel fields<sup>37</sup> or mesoscopic superconducting disks.<sup>8,12</sup> In this section we study the magnetic behavior of superconducting samples of different sizes, in particular we cover the sample size region where a transition from a mesoscopic to a bulk behavior takes place.

Figure 5 shows the dc-magnetic behavior of superconducting square samples of different sizes with S-I boundary condition. The behavior of Fig.5(a) is typical of the macroscopic samples that we have studied in the previous section, however if we decrease the sample size to the mesoscopic region the continuous behavior disappears and some magnetization maxima followed by discontinuous jumps appear (see Figs.5(b) and (c)).

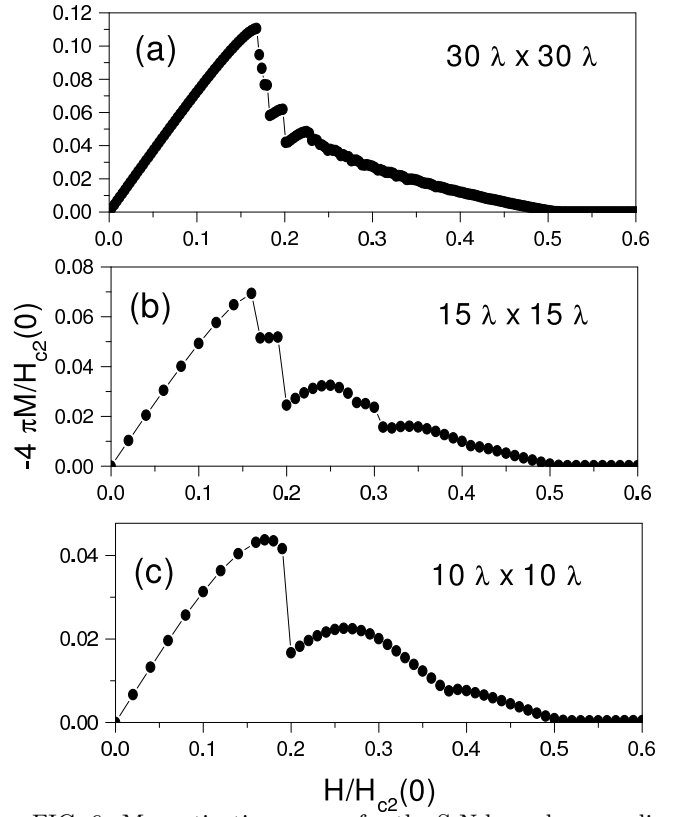


FIG. 6. Magnetization curves for the S-N boundary condition and  $\kappa = 2$ . We show the magnetic curves at different sample sizes from the macroscopic to the mesoscopic-like behavior: (a)  $30\lambda \times 30\lambda$ , (b)  $15\lambda \times 15\lambda$  and (c)  $10\lambda \times 10\lambda$ .

We find that the discontinuities in the magnetization correspond to the penetration of new vortices into the sample, this will be discussed in detail in Sec.IVB.

If we change the boundary condition and we use the ‘S-N’ condition we find, as it is shown in Figure 6, a different mesoscopic behavior: there is an appreciable decrease in the number of magnetization maxima and the transition between the states of the system with a different number of vortices seems more continuous. In other words, for the same sample size, fewer vortex penetration events are needed to arrive to the normal state. The decrease in the number of entrance events for the S-N boundary in mesoscopic samples is related to the fact that this boundary condition allows less vortices inside the sample, as discussed in the previous section. The fact that the S-N interface needs a larger shielding distance,  $\delta_{SN} > \delta_{SI}$ , has clearly stronger consequences in the magnetic behavior of a mesoscopic sample. At the same magnetic field the mean magnetization values of the Meissner state are lower in the S-N case than in the S-I case as can be observed comparing Figures 5(c) and 6(c). In general a mesoscopic sample with a boundary corresponding to  $0 < b < \infty$  in Eq.(6), will have a magnetization behavior in between the two limiting cases of Fig. 5 and Fig. 6.

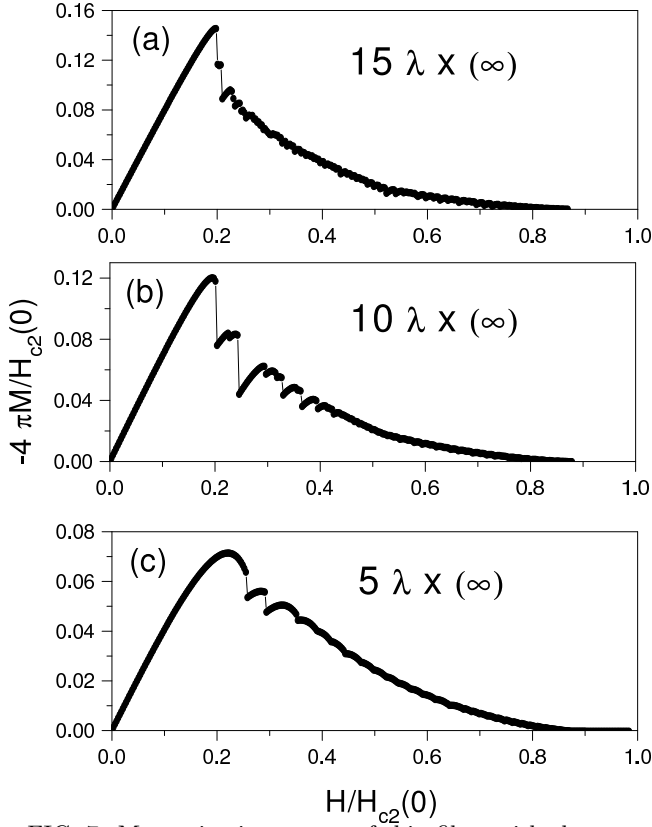


FIG. 7. Magnetization curves of thin films with the external magnetic field applied parallel to the film. The curves are generated for decreasing thicknesses of the film and using the S-I boundary condition for  $\kappa = 2$ . (a)  $15\lambda \times \infty$ , (b)  $10\lambda \times \infty$  and (c)  $5\lambda \times \infty$ .

The changes observed in the magnetization curves when going from the macroscopic to the mesoscopic behavior are quite general and do not depend on the sample geometry. We also study the magnetic behavior of a thin film with the field parallel to its faces. In this case there is only one relevant dimension, the thickness of the film ( $d$ ). We work here in the case  $d > \lambda$ . Figure 7 shows the magnetic behavior of thin films with different thickness obtained using the S-I boundary condition. We observe that in this case the discontinuities in the magnetization curves appear at smaller film thickness and that they are less important than in squares samples, possibly because vortices in a mesoscopic square sample are more confined than in thin films of the same linear size. We have also done numerical calculations of the magnetic behavior in thin films using the S-N boundary condition (see Figure 8). In particular Figure 8(c) shows that for very small film thickness there is a continuous change in magnetization without the jagged structure observed in Fig.8(a-b). In this case vortex lines do not penetrate the sample and the superconducting state disappears gradually. This behavior is also present when we use the S-I boundary condition but it is necessary to explore lower sample sizes than the one shown in the corresponding figures.

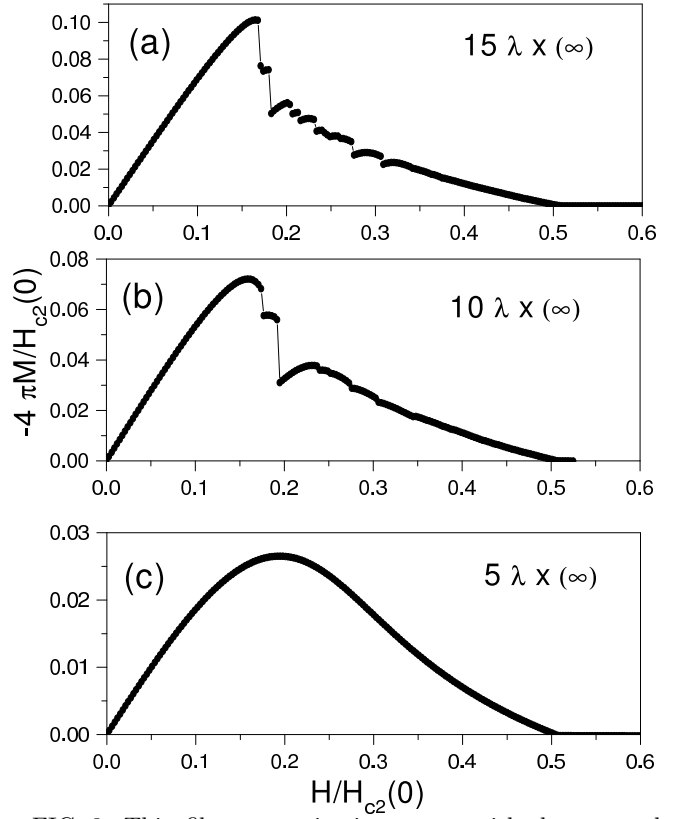


FIG. 8. Thin film magnetization curves with the external field applied in the same geometry of Figure 7 but using the S-N condition: (a)  $15\lambda \times \infty$ , (b)  $10\lambda \times \infty$  and (c)  $5\lambda \times \infty$ . As it is observed for samples sizes as low as  $5\lambda \times \infty$ , there is a continuous transition to the normal state.

## B. Multiple penetration fields in mesoscopic samples

The behavior of the magnetization in mesoscopic type II samples is characterized by maxima followed by discontinuous jumps as a function of the external magnetic field. In Figure 9 we show in detail the case for a sample of size  $10\lambda \times 10\lambda$  and  $\kappa = 2$ . At the same time we plot the total number of vortices inside the sample,  $N_v = \frac{1}{\Phi_0} \oint (A + \frac{J_s}{|\Psi|^2}) dl$ . We see that each discontinuous jump in  $M(H)$  corresponds to an increase of  $\Delta N_v = 4$  in the number of vortices. These jumps occur at successive magnetic fields  $H_{pi} = H_{p1}, H_{p2}, H_{p3}, \dots$ , which are indicated in the figure. In the regions of  $H_{pi} < H < H_{p(i+1)}$  the number of vortices  $N_v$  is constant. Therefore the only penetration events occur at  $H_{pi}$ , when one vortex enters in each of the four sides of the square sample. In the region of constant vorticity,  $H_{pi} < H < H_{p(i+1)}$ , one may think that no vortices enter the sample because they feel a surface barrier which is enhanced by the repulsion force exerted by the vortices already inside the sample.



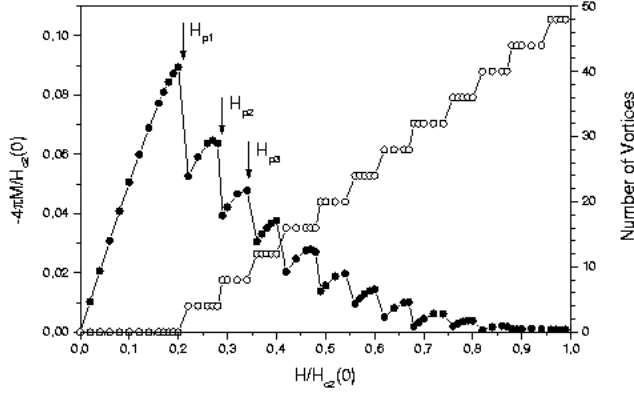


FIG. 9. Magnetization curves for a mesoscopic  $10\lambda \times 10\lambda$  square sample using the S-I boundary condition for  $\kappa = 2$ . In the right scale the number of vortices  $N_v$  is shown.

To analyze this effect, let us extend the simple London approximation model of Bean and Livingston for the surface barrier to the case when there are extra vortices inside the sample and near the boundary. In the London approach, the Gibbs free energy ( $G$ ) of a vortex line located a distance  $x$  from the sample surface can be calculated as:<sup>5,25</sup>

$$G = \frac{\Phi_o}{4\pi} [H_a \exp(-\frac{x}{\lambda}) - \frac{1}{2} \frac{\Phi_o}{2\pi\lambda^2} K_o(\frac{2x}{\lambda}) + H_{c1} - H_a] \quad (12)$$

where  $H_a$  is the external magnetic field and  $K_o$  is the modified Bessel function of the second kind. In normalized units the above expression reads:

$$\frac{4\pi G}{H_{c2}\Phi_o} = [H_a \exp(-\frac{x}{\lambda}) - \frac{1}{2\kappa^2} K_o(\frac{2x}{\lambda}) + \frac{\ln \kappa}{2\kappa^2} - H_a] \quad (13)$$

where we have used the relation  $H_{c1} = (\ln \kappa)/2\kappa^2 H_{c2}$ . The first term of Equations (12) and (13) is related with the repulsive interaction between the vortex line and the external field, the second term describes the attraction between the vortex and the surface currents, this term is usually interpreted as the interaction with an image vortex<sup>5,25</sup> and the third term is the vortex self energy.

The above expressions are valid when there are no vortices inside the sample. If there are vortices located inside the sample, some additional terms due to the interaction between the vortices are needed. In the following we will assume that there is only one vortex inside the sample located at position  $l$  and that we are analysing the Gibbs free energy in the same line perpendicular to the sample surface. If  $l$  is small, the new vortex that is trying to enter the sample now feels two additional terms. The first term is the repulsive force between the vortices and the second is the attractive interaction with the image of the vortex located inside the sample. The last term is needed in order to take into account the perturbation of the

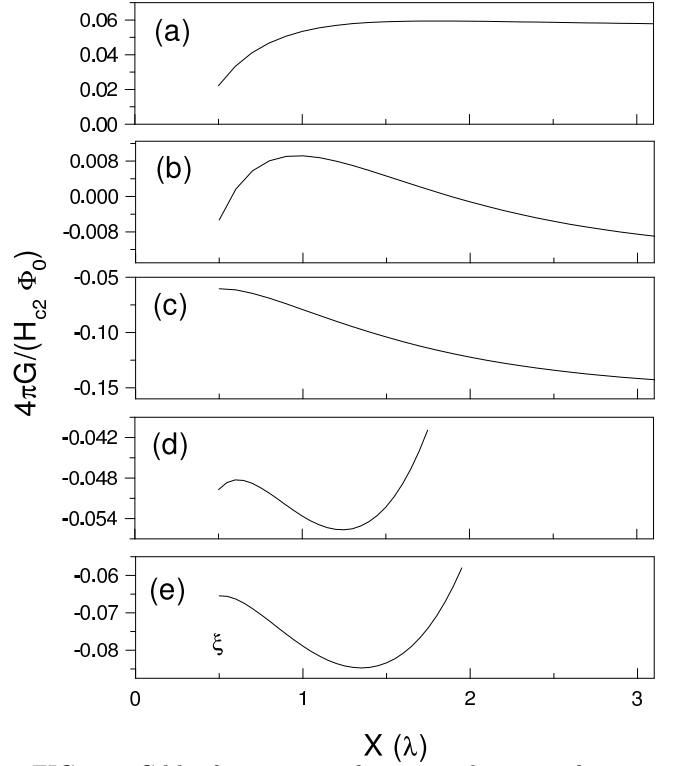


FIG. 10. Gibbs free energy of a vortex line as a function of the distance  $x(\lambda)$  from the sample surface. We have used Equation (12) for (a)  $H = 0.03H_{c2}$ , (b)  $H = 0.1H_{c2}$ , (c)  $H = 0.24H_{c2}$  and Equation (13) for (d)  $H = 0.24H_{c2}$  and (e)  $H = 0.28H_{c2}$ .

vortex already inside the sample because of its proximity to the surface. Both contributions are more important in mesoscopic superconductors as we will show below. The free energy that gives the correct force expression is:

$$\frac{4\pi G}{H_{c2}\Phi_o} = H_a \exp(-\frac{x}{\lambda}) - \frac{1}{2\kappa^2} K_o(\frac{2x}{\lambda}) + \frac{\ln \kappa}{4\kappa^2} - H_a + \frac{1}{\kappa^2} K_o(\frac{l-x}{\lambda}) - \frac{1}{\kappa^2} K_o(\frac{l+x}{\lambda}) \quad (14)$$

Equations (13) and (14) are approximate expressions and have the limitation that they are not valid near the sample surface, then we will only use it for  $x > \xi$ . It is useful to note that in a more exact treatment we should obtain that  $G \rightarrow 0$  when  $x \rightarrow 0$  because the Gibbs free energy of a vortex located outside the sample must be zero.

Figures 10(a), 10(b) and 10(c) were generated using Equation (13) for  $\kappa = 2$ . The free energy of the vortex depends on both the applied magnetic field and the distance to the surface. For  $H < H_{c1}$  the free energy associated with a vortex is positive at all  $x$  values, as it is shown in Figure 10(a), vortices are then thermodynamically unstable inside the superconductor and there is an energy cost associated with the vortex entrance. The thermodynamic condition for vortex penetration is not fulfilled until  $H > H_{c1}$ , when the free energy of a vortex located well inside the superconductor becomes negative, see Figure 10(b). However, Figure 10(b) also

shows that because of the attractive interaction between the vortex and the surface currents a barrier to vortex entrance appears nears the surface. This is the “Bean-Livingston” surface barrier originated by the screening currents. Taking into account Equation (13) it is possible to estimate  $H_p$  as the magnetic field for which the expression  $(\partial G/\partial x)_{x=\xi}$  becomes negative, i.e. when the maximum of  $G(x)$  moves inside the region  $x < \xi$ . This condition is fulfilled at  $H_p = \frac{\sqrt{2}}{2}H_c$  ( $H_p \approx 0.24H_{c2}$  in Figure 10(c)). At  $H = H_p$  some vortices penetrate the sample and the free energy associated with the entrance of a new vortex now must be calculated using an analogous to Equation (14), the exact expression depends on the number of vortices and their location inside the sample. Considering only one vortex located at  $x = l = 3\lambda$  and using Equation (14) we have calculated the free energy just after the first vortex entrance ( $H > 0.24H_{c2}$ ), the results are shown in Figure 10(d). Observe that the free energy changes considerably from Figure 10(c) to figure 10(d). Now there are three relevant regions: i) near  $x = 3\lambda$ , there is a region where the Gibbs free energy increases with increasing  $x$ , the strong repulsive interaction with the vortex inside the sample dominates; ii) there is an intermediate region where  $G$  decreases at increasing  $x$ , this means that a vortex located in this region will be pulled inside the sample, it is possible to allocate vortices in this region and there is also a region iii) near the sample surface that repels vortex entrance,  $G$  increases for increasing  $x$ . The existence of regions ii) and iii) means a reinforcement of the surface barrier induced by vortex penetration and allows magnetic field intervals of metastable states. This energy barrier reinforcement due to vortex entrance is more important in mesoscopic superconductors because, in small samples, vortices are confined by the potential well generated by the sample surface and even a vortex fixed in the center of the sample is very close to the surface. For example in an  $10\lambda \times 10\lambda$  square sample, vortices are constrained to be located around the center of the sample at  $x = 5\lambda$ , because of its interaction with the surface currents. As a consequence vortices stay at  $x \approx 5\lambda$  generating a new surface barrier and it is necessary an important magnetic field increase to allow new vortex penetration. For macroscopic samples the situation is quite different, there is a nearly continuous vortex penetration. In macroscopic samples the vortices that are inside the sample are not confined and they do not have serious restrictions in their movement since they can be allocated very far from the surface. In this case, a small increase of the magnetic field is enough to accommodate new vortex lines, as can be observed in Figure 5(a).

From the analysis of Figure 9 and the previous discussion we can conclude that in mesoscopic samples there are preferred values of magnetic field for vortex penetration, in this case the process of vortex entrance is discontinuous in contrast with the continuous macroscopic regime. This behavior is a consequence of the barrier to vortex

entrance that appears after each penetration event. In this way we can define a second penetration field  $H_{p2}$ , a third penetration field  $H_{p3}$  and so on. We observe that after increasing the size of the sample the vortex penetration becomes continuous ( $H_{p3} \rightarrow H_{p2} \rightarrow H_p$ ).

The exact delimitation of the macroscopic and mesoscopic regimes depends on the geometry of the sample. We will now study in detail the behavior of a thin film because is a simpler case with only one significant length scale. The size dependence of the penetration fields  $H_p, H_{p2}, H_{p3}$  obtained numerically from the TDGL equations in a thin film using the S-I boundary condition are summarized in Figure 11(a). For  $d > 15\lambda$  a continuous vortex penetration is observed, this is the region of a macroscopic behavior. The mesoscopic region is located at  $2\lambda \lesssim d \lesssim 15\lambda$  in which several penetration fields  $H_{pi}$  can be distinguished. For  $d < 2\lambda$  there is a gradual transition to the normal state without vortices. Figure 11(b) shows the sample size dependence of the first, second and third penetration field of thin films using an S-N boundary condition. For the S-N boundary the scales are shifted to larger sizes since the shielding length is larger ( $\delta_{SN} > \delta_{SI}$ ), as we discussed before. The macroscopic behavior appears at  $d > 18\lambda$ , the mesoscopic region is located between  $5\lambda \lesssim d \lesssim 18\lambda$  and for  $d < 5\lambda$  a continuous transition to the normal state appears.

It is interesting to note that  $H_p$  is size dependent in the mesoscopic region. This size dependence can be explained by considering in Equation (13) the effect of two surfaces that are separated by a small distance  $d$ . The term generated by the magnetic field  $H \exp(-x/\lambda)$  now becomes  $H \cosh[(x-d)/\lambda] / \cosh(d/\lambda)$  due to the proximity of the other surface, the magnetic force that pulls the vortex inside the sample decreases when the film thickness ( $d$ ) decreases. The image term also changes because the vortex lines that are trying to enter the sample are now near both surfaces and new image lines are necessary in order to satisfy the boundary condition at both surfaces. The application of the image method to parallel surfaces gives an infinite number of images, but the net effect is the appearance of an attractive interaction to the new surface. Then, in the mesoscopic region, there is also a decrease in the net attractive image force. If we consider only three relevant terms in the image forces, the normalized force  $f = (4\pi/\Phi_0 H_{c2})\lambda(\delta G/\delta x)$  that feels a vortex line that is trying to enter when the sample is in the Meissner state can be estimated by:

$$f = H_a \frac{\sinh(\frac{x-d/2}{\lambda})}{\cosh(d/2\lambda)} + \frac{1}{\kappa^2} K_1\left(\frac{2x}{\lambda}\right) - \frac{1}{\kappa^2} K_1\left(\frac{2d-2x}{\lambda}\right) + \frac{1}{\kappa^2} K_1\left(\frac{2d+2x}{\lambda}\right) \quad (15)$$

where  $d$  is the thickness of the film and we have chosen  $f$  positive when it repels the vortex entrance. As we analyzed before,  $H_p$  is usually obtained from  $f|_{x=\xi} = 0$ .

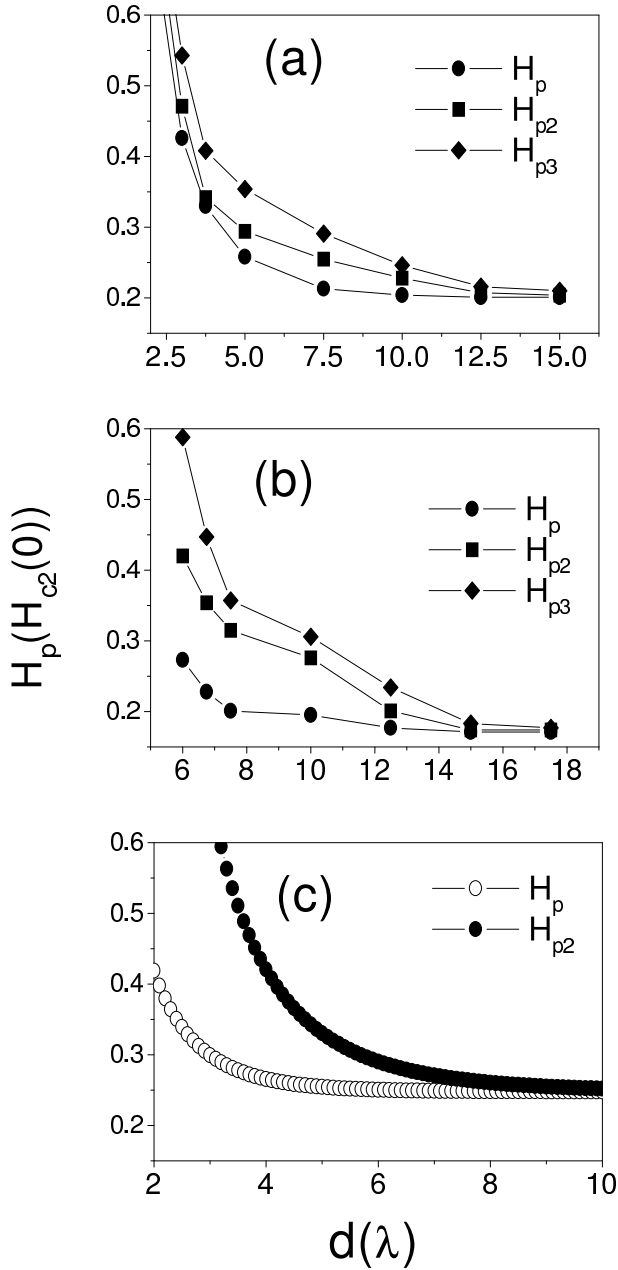


FIG. 11. Penetration fields obtained from the magnetic curves shown in Figures 11 and 12. We plot the first, second and third penetration fields at different film thickness for (a) S-I and (b) the S-N boundary condition.  $H_{p3} \neq H_{p2} \neq H_p$  is typical of a mesoscopic behavior. For large film thickness, in the region of the macroscopic behavior, a continuous entrance of vortices is recovered ( $H_{p3} \rightarrow H_{p2} \rightarrow H_p$ ). Figure (c) shows an estimation of  $H_p$  and  $H_{p2}$  using the image method and considering the influence of the sample size in the field profile.

This condition leads to the following expression for  $H_p$ :

$$H_p = \frac{[K_1(\frac{2\xi}{\lambda}) - K_1(\frac{2d-2\xi}{\lambda}) + K_1(\frac{2d+2\xi}{\lambda})] \cosh(\frac{d}{2\lambda})}{\kappa^2 \sinh(\frac{d-2\xi}{2\lambda})} \quad (16)$$

We have evaluated this behavior of  $H_p(d)$  in Figure

11(c). As it can be observed, when we decrease the thickness of the film the repulsive magnetic force decreases faster than the attractive term, and the  $H_p$  value increases. In Figure 11(c) we also estimate the behavior of the second penetration field  $H_{p2}$  as a function of the sample size. The approximate expression used was obtained including in the Equation (15) the extra terms related with the presence of a vortex line inside the sample as we did in Equation (14). For simplicity we have considered one vortex located at the middle of the sample at  $x = d/2$ . Under this condition  $H_{p2}$  becomes:

$$H_{p2} = [K_1(\frac{2\xi}{\lambda}) - K_1(\frac{2d-2\xi}{\lambda}) + K_1(\frac{2d+2\xi}{\lambda}) + K_1(\frac{d-2\xi}{2\lambda}) + K_1(\frac{d+2\xi}{2\lambda}) - K_1(\frac{3d+2\xi}{2\lambda})] \frac{\cosh(\frac{d}{2\lambda})}{\kappa^2 \sinh(\frac{d-2\xi}{2\lambda})} \quad (17)$$

this expression also reproduces the  $H_{p2}$  sample size dependence observed in the numerical simulations.

## V. SUMMARY

We have presented results on the study of the magnetization curves and the surface barrier for type I and type II superconductors. Our results show that the strength of the surface barrier depends on the boundary. If the interface is of the S-I type, the vortices that enter find a higher barrier for penetration since the order parameter at the surface has to go through an intermediate state of  $\Psi = 0$ , while for the S-N boundary condition the vortex entrance occurs more smoothly since the  $\Psi = 0$  condition is already fulfilled by the interface. In this later case the surface barrier is only due to the Meissner shielding currents and the penetration field  $H_p$  agrees well with the Bean-Livingston value, while in the S-I case  $H_p$  is higher and dependent on  $\kappa$ . Superconductors with more realistic boundary conditions should lie in between these two cases.

We also characterized the reinforcement of the surface barrier due to the presence of vortex lines inside the sample in mesoscopic superconductors. We show that these new barriers allow for the existence of metastable states of constant vorticity as a function of magnetic field. Each metastable state becomes unstable at the  $i$ -th penetration field  $H_{pi}$  in which one vortex enters in each side of the sample and the magnetization has a discontinuous jump. We study the magnetization curves at different sample dimensions and we obtain the sample size dependence of the first, second and third penetration fields. We finally show that for sufficiently large sample sizes the continuous macroscopic regimen is recovered, i.e.  $H_{p3} \rightarrow H_{p2} \rightarrow H_p$ .

## ACKNOWLEDGMENTS

We acknowledge helpful discussions with Arturo López and Niels Grønbech-Jensen. A.D.H. acknowledges Oscar Arés and C. Hart for useful comments and help and the Centro Latino-Americano de Física (CLAF) for financial support. D.D. acknowledges support from Conicet and CNEA (Argentina). We also acknowledge the financial support for this project from ANPCyT and Fundación Antorchas.

- 
- <sup>1</sup> O. Buisson, P. Gandit, R. Rammal, Y. Y. Wang and B. Pannetier, Phys. Lett. A **150**, 36 (1990). O. Buisson, Ph.D. Thesis, L' Université Joseph Fourier, Grenoble, 1990.
  - <sup>2</sup> A. K. Geim, I. V. Grigorieva, S. V. Dubonos, J.G.S. Lok, J.C. Maan, A.E. Filipov, and F.M. Peeters, Nature **390**, 259 (1997); A. K. Geim, S. V. Dubonos, J.G.S. Lok, M. Henini and J.C. Maan, Nature **396**, 144 (1998).
  - <sup>3</sup> C. A. Bolle, V. Aksyuk, F. Pardo, P. L. Gammel, E. Zeldov, E. Bucher, R. Boie, D. J. Bishop and D.R. Nelson, Nature **399**, 43 (1999).
  - <sup>4</sup> A. K. Geim, S. V. Dubonos, I. V. Grigorieva, F. M. Peeters and V. A. Schweigert, Nature **407**, 55 (2000).
  - <sup>5</sup> C. P. Bean and J. D. Livingston, Phys. Rev. Lett. **12**, 14 (1964).
  - <sup>6</sup> Y. Enomoto and K. Okada, J. Phys. Cond. Matter **9**, 10203 (1997).
  - <sup>7</sup> E. B. Sonin and K. B. Traito, Phys. Rev. B, **50**, 13547 (1994).
  - <sup>8</sup> P. Singha Deo, V. A. Shweigert, F. M. Peeters and A. K. Geim, Phys. Rev. Lett. **79**, 4653 (1997).
  - <sup>9</sup> V. A. Shweigert, F. M. Peeters and P. Singha Deo, Phys. Rev. Lett. **81**, 2783 (1998).
  - <sup>10</sup> V. A. Shweigert and F. M. Peeters, Phys. Rev. B **57**, 13817 (1998).
  - <sup>11</sup> V. A. Shweigert and F. M. Peeters, Phys. Rev. Lett. **83**, 2409 (1999).
  - <sup>12</sup> V. A. Shweigert and F. M. Peeters, Phys. Rev. B **60**, 3084 (1999).
  - <sup>13</sup> A. V. Kuznetsov, D. V. Eremenko, V. N. Trofimov, Phys. Rev. B **59**, 1507 (1999).
  - <sup>14</sup> P. Singha Deo, V. A. Shweigert and F. M. Peeters, Phys. Rev. B **59**, 6039 (1999).
  - <sup>15</sup> A. Schmid, Phys. Condens. Matter **5**, 302 (1966); C. R. Hu and R. S. Thompson, Phys. Rev. B **6**, 110 (1972); A. T. Dorsey, Phys. Rev. B **46**, 8376 (1992).
  - <sup>16</sup> L. P. Gorkov and G. M. Eliashberg, Soviet Phys.-JETP **27**, 328 (1968).
  - <sup>17</sup> H. Frahm, S. Ulah and A. T. Dorsey, Phys. Rev. Lett. **66**, 3067 (1991).
  - <sup>18</sup> F. Liu, M. Mondelo and N. Goldenfeld, Phys. Rev. Lett. **66**, 3071 (1991).
  - <sup>19</sup> R. Kato, Y. Enomoto and S. Maekawa, Phys. Rev. B **47**, 8016 (1993).
  - <sup>20</sup> M. Machida and H. Kaburaki, Phys. Rev. Lett. **71**, 3206 (1993); Phys. Rev. B, **50**, 1286 (1994).
  - <sup>21</sup> I. Aranson, M. Gitterman and B. Ya. Shapiro, Phys. Rev. B, **51**, 3092 (1995); I. Aranson, B. Ya. Shapiro and V. Vinokur, Phys. Rev. Lett. **76**, 142 (1996); I. Aranson, and V. Vinokur, Phys. Rev. Lett. **77**, 3208 (1996).
  - <sup>22</sup> J. J. Vicente Álvarez, D. Domínguez and C. A. Balseiro, Phys. Rev. Lett. **79**, 1373 (1997).
  - <sup>23</sup> W. D. Groop, H. G. Kaper, G. L. Leaf, D. M. Levine, M. Palumbo and V. M. Vinokur, J. Comp. Phys. **123**, 254 (1996).
  - <sup>24</sup> It is possible to extend the mean field dynamics of TDGL by adding Langevin noise terms both for  $\Psi$  and  $A$  in Equations (1-2). This leads to configurations which in equilibrium have a Boltzmann probability proportional to  $e^{-\mathcal{F}/kT}$  with  $\mathcal{F}$  the Ginzburg-Landau free energy. This can be relevant for describing thermally activated vortex penetration events in high temperature superconductors and more importantly for the behavior near the phase transitions in the high  $T_c$  vortex phase diagram (vortex lattice melting, vortex glasses, etc.). See for example A. T. Dorsey and M.P.A. Fisher, Phys. Rev. Lett. **68**, 694 (1992).
  - <sup>25</sup> P. G. de Gennes: Superconductivity of metals and alloys (Adison-Wesley) 1989.
  - <sup>26</sup> J. O. Indekeu and J. M. J. van Leeuwen, Phys. Rev. Lett. **75**, 1618 (1995).
  - <sup>27</sup> Only out of equilibrium we find that structures of coexisting normal and superconducting phase can be nucleated, as was found in Ref. 17,18.
  - <sup>28</sup> R. E. Goldstein, D. P. Jackson and A. T. Dorsey, Phys. Rev. Lett. **76**, 3818 (1996), A. T. Dorsey and R. E. Goldstein, Phys. Rev. B **57**, 3058 (1998).
  - <sup>29</sup> H. Bokil and O. Narayan, Phys. Rev. B **56**, 11195 (1997).
  - <sup>30</sup> V. L. Ginzburg, Sov. Phys. JETP **7**, 78 (1958).
  - <sup>31</sup> J. Matricon and D. Saint-James, Phys. Lett. **24A**, 241 (1967).
  - <sup>32</sup> L. Kramer, Phys. Rev. **170**, 475 (1968).
  - <sup>33</sup> H. J. Fink and A. G. Presson, Phys. Rev. **182**, 498 (1969).
  - <sup>34</sup> L. Kramer, Z. Physik, **259**, 333 (1973).
  - <sup>35</sup> A. J. Dolgert, S. J. Di Bartolo and A. T. Dorsey, Phys. Rev. B **53**, 5650 (1996).
  - <sup>36</sup> D. Vodolazov, Phys. Rev. B **62**, 8691 (2000).
  - <sup>37</sup> C. Bolech, G. C. Buscaglia and A. López, Phys. Rev. B, **52**, R15719 (1995).